AIP | Applied Physics Letters

A subwavelength near-infrared negative index material

Xuhuai Zhang, Marcelo Davanço, Yaroslav Urzhumov, Gennady Shvets, and Stephen R. Forrest

Citation: Applied Physics Letters **94**, 131107 (2009); doi: 10.1063/1.3110957
View online: http://dx.doi.org/10.1063/1.3110957
View Table of Contents: http://scitation.aip.org/content/aip/journal/apl/94/13?ver=pdfcov
Published by the AIP Publishing

A subwavelength near-infrared negative index material

Xuhuai Zhang,[1] Marcelo Davanço,[1] Yaroslav Urzhumov,[2] Gennady Shvets,[2] and Stephen R. Forrest[1,3,a)]
[1]*Department of Physics, University of Michigan, Ann Arbor, Michigan 48109-1040, USA*
[2]*Department of Physics, University of Texas, Austin, Texas 78712-0264, USA*
[3]*Department of Electrical Engineering and Computer Science, University of Michigan, Ann Arbor, Michigan 48109-2122, USA*

(Received 7 December 2008; accepted 6 March 2009; published online 2 April 2009)

A single layer of a subwavelength negative index material (NIM) operating at a wavelength of 1 μm is demonstrated. The geometrical parameters of the nanostructure are determined by characterizing its optical transmission spectrum. We show through photonic band calculations that these parameters give rise to a negative index in a corresponding bulk NIM. The fabrication inaccuracies in the dielectric spacer thickness that are likely to be introduced in a prism composed of multiple layers of this structure are shown through full-wave simulations to be within a range that preserves its negative refractive behavior. © *2009 American Institute of Physics*.
[DOI: 10.1063/1.3110957]

Negative index materials (NIMs)[1,2] have recently been reported at near-infrared or higher optical frequencies. Unlike their microwave counterparts that are substantially subwavelength, optical NIMs typically have a large unit cell size that is approximately half of the wavelength of operation in at least one dimension, which makes the application of the effective medium theory problematic.[3,4] For the commonly reported "fishnet" structure,[5] for example, its large transverse dimension is dictated by the high excitation frequency of the gap surface plasmon polariton,[6] which is responsible for the magnetic resonance that gives rise to its negative index of refraction.[4]

More recently, a near-infrared NIM structure was proposed[7,8] whose unit cell, extending infinitely along the $\hat{z}$ direction is shown in Fig. 1(a). It consists of a pair of 20 nm thick by 100 nm wide Au strips, separated from a 20 nm thick central continuous Au layer by 15 nm thick dielectric spacers. For transverse magnetic polarized ($\mathbf{H}=H_z\hat{z}$) electromagnetic waves propagating along the $\hat{x}$ direction in the x-y plane, the structure has been theoretically shown to possess a bulk negative index that was tested using full-wave simulations of refraction of hypothetical prisms consisting of multiple layers of this structure.[8] The unit cell is subwavelength ($\sim\lambda/7$) in both the $\hat{x}$ and $\hat{y}$ directions where there are field variations, making it desirable for applications requiring a large optical incidence angle.[8] Here, we describe the fabrication of this structure, characterize its optical transmission, and examine the influence of fabrication error on its potential bulk negative index properties.

The single layer NIM was fabricated on a glass substrate using electron-beam lithographic patterning of the submicron features. Several 100×100 μm^2 patterns were written with varying Au strip widths ranging from 70 to 120 nm. Fiducial marks for alignment were defined in the first strip layer photoresist [poly(methyl methacrylate) 495K, MicroChem, Corp.] step. Following the deposition of the first layer of 20 nm thick Au at 5 Å/s and lift-off of the photoresist in acetone, an approximately 40 nm thick layer of cyclotene diluted in mesitylene was spun onto the sample surface and cured in a nitrogen oven at 250 °C for 1 h. The root mean square roughness of the polymer surface was measured with an atomic force microscope to be <5 nm, as shown in Fig. 1(b). The dielectric layer was then etched in a CF_4:O_2 plasma to attain a thickness of 10–20 nm. Optical lithogra-

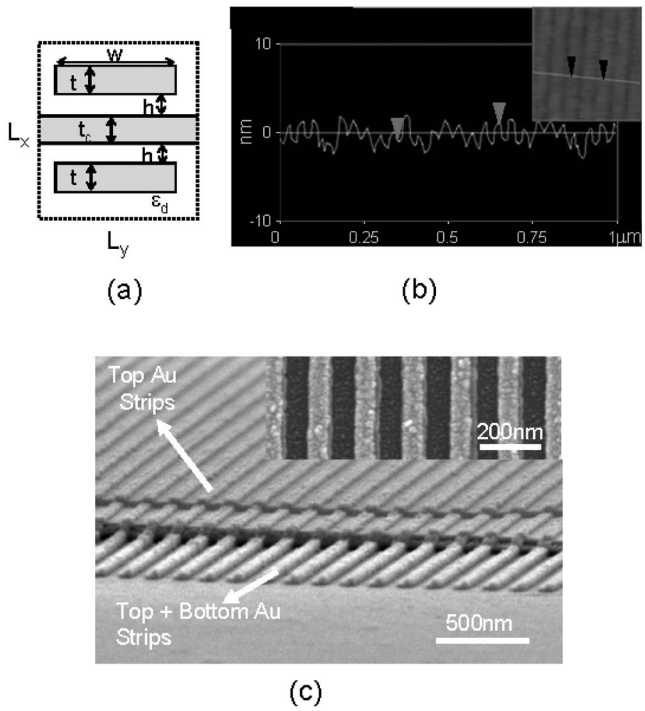

FIG. 1. (a) The unit cell. Lattice constants $L_x=L_y=150$ nm, Au strip and central layer thicknesses $t=t_c=20$ nm, strip width $W=100$ nm, and spacer thickness $h=15$ nm. Gold strips and the central metallic layer are embedded in a polymer dielectric (cyclotene). (b) Atomic force microscope profile after planarization by the cured polymer on top of the Au grating pattern. The peak-to-valley roughness is 4.3 nm. Inset: The atomic force microscope image of the grating covered by the cured polymer where the white line transverse to strips shows the cross section analyzed, and the marks correspond to their positions in (b). (c) SEM image of a completed structure. Inset: Top strips on top of the bottom strips at the edge of the pattern showing the alignment between them where the central metallic layer is absent.

a)Electronic mail: stevefor@umich.edu.

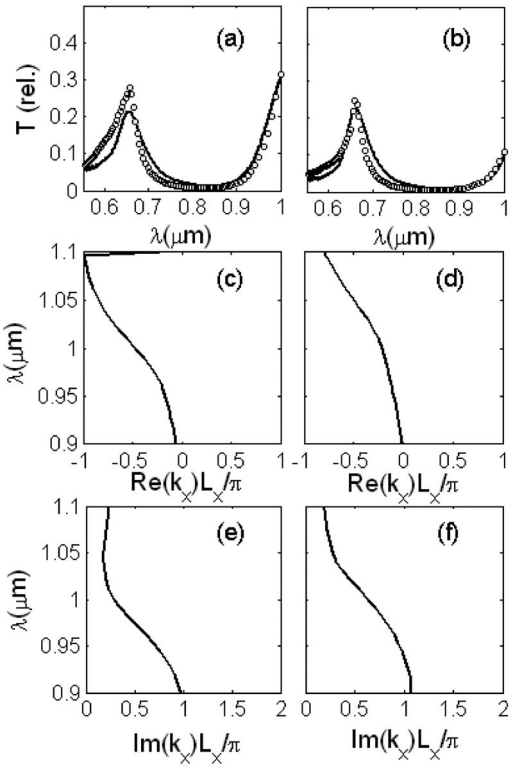

FIG. 2. (a) and (b) Transmission spectra for the NIM layers in Fig. 1. Continuous lines are experimental data; open circles are simulated results for structures with metal layer thicknesses $t=t_c=22$ nm, top and bottom spacer thicknesses $h_{top}=15$ nm and $h_{bot}=9$ nm, respectively. Strip widths: (a) $W=105$ nm and (b) $W=110$ nm. [(c)–(f)] Calculated band structure of the dominant Bloch mode assuming the geometrical parameters of (a) and (b), respectively. Transmission spectra and band structure of the same geometrical parameters are in the same column.

phy was used to define 100×100 μm^2 Ti(2 nm)/Au(20 nm) patches that covered the grating patterns, corresponding to the central metallic layer. Here the Ti layer enhances the adhesion of the Au to the dielectric. Next, a second 40 nm thick dielectric layer was spun on and etched as above. The top strip layer consisting of 20 nm thick Au was defined with electron-beam lithography, followed by a second metal lift-off step. Scanning electron microscope (SEM) images of samples shown in the inset of Fig. 1(c) indicate that alignment within 20 nm between top and bottom strip layers was achieved. The completed structure is shown in Fig. 1(c).

Transmittance spectra were obtained by illuminating the square patterns with a ~20 μm diameter, broadband supercontinuum laser beam obtained by coupling the output of a Nd-YAG pulsed laser into a photonic crystal fiber. The transmitted beam was analyzed with a spectrometer. Low-numerical aperture and visible/near-infrared achromatic objectives with long working distances were used for collimating and focusing the broadband light. Spectra (relative to transmission through glass) for two patterns with an SEM-estimated strip width of 100 nm are shown in Figs. 2(a) and 2(b). Also shown is the transmittance calculated using the Au dielectric constant,[9] and the metal and dielectric layer thicknesses and strip widths measured for the samples studied. The refractive index for the dielectric layers was 1.56 from ellipsometry, and 1.45 for the glass substrate. The thicknesses of metal and dielectric layers and strip widths were adjusted within reasonable limits to yield quantitatively good fits to the measured transmission spectra in Figs. 2(a) and 2(b). That is, we used Au strip and central layer thicknesses of $t=t_c=22$ nm, $h_{top}=15$ nm, and $h_{bot}=9$ nm for the top and bottom dielectric spacer layers, and strip widths $W=105$ and 110 nm, respectively. These dimensions are compiled in Table I along with calculated errors, which are defined as the ratio of the maximum absolute deviation to the nominal value.

TABLE I. Nominal and experimentally determined dimensions of the negative index material structure in Fig. 1. Relative fabrication errors of the various dimensions are shown.

	Au layer thicknesses	Au strip widths	Top spacer thickness	Bottom spacer thickness
Nominal	20 nm	100 nm	15 nm	15 nm
Pattern 1	22 nm	105 nm	15 nm	9 nm
Pattern 2	22 nm	110 nm	15 nm	9 nm
Relative error	10%	10%	40%	40%

We have shown[8] that for an arbitrary low-loss unit cell, the bulk effective refractive index n_{eff} that is consistent with Snell's law is given by the result of photonic band calculations following: $n_{eff}=(k/k_0)\mathrm{sgn}[\partial\omega/\partial\,\mathrm{Re}(k)]$, provided that a single Bloch band dominates, the losses are small, and the unit cell is small compared to the vacuum wavelength. Here, k is the wave vector of the dominant band in the first Brillouin zone, k_0 is the free-space wave number, and ω is the angular frequency. The dispersion relation of the dominant Bloch band for the unit cells corresponding to patterns[10] 1 and 2 in Table I are shown in Figs. 2(c)–2(f). In both cases, a low-loss negative index band at wavelengths $\lambda>1$ μm, characterized by $k[\partial\omega/\partial\,\mathrm{Re}(k)]<0$, is apparent. The slight redshift of this band relative to the calculations in Ref. 8 is due to the fabrication errors. Accordingly,[8] the existence of the low-loss band, together with the subwavelength feature size, provides a sufficient condition for negative refraction to occur.

Table I shows that of all the fabrication errors, the thicknesses of the dielectric spacer layers have the largest relative deviation due to their small dimensions and inaccuracies in the plasma etching process. Although we have established the negative index for the bulk NIM through band calculations, a bulk NIM fabricated with a layer-by-layer process[11] will nevertheless inevitably have such random fabrication errors in the dielectric spacer thicknesses. It is of interest to examine how the negative refractive behavior of the bulk will be affected by this randomness. We have, therefore, simulated[8] a 3 dimensional prism composed of the unit cells of Fig. 1(a), where the angle of the hypotenuse is 18°. The dielectric spacer thickness (and hence the vertical position of each metal strip layer) is subject to a fabrication error that is simulated by a random variable in the range from −7.5 to 7.5 nm. Other sources of fabrication errors are neglected since they are considerably smaller in relative magnitude. In the simulation, the TEM_{00} mode of a parallel metal plate waveguide is normally incident upon the bottom of the prism.

A representative field plot at $\lambda=970$ nm is shown in Fig. 3(a). In most situations, there are two far-field beams. The angular positions of the transmitted beams are used to determine the refractive indices, which are plotted in Fig. 3(b), together with the index of refraction calculated from the band structure of the unit cell of Fig. 1(a).[8] The different

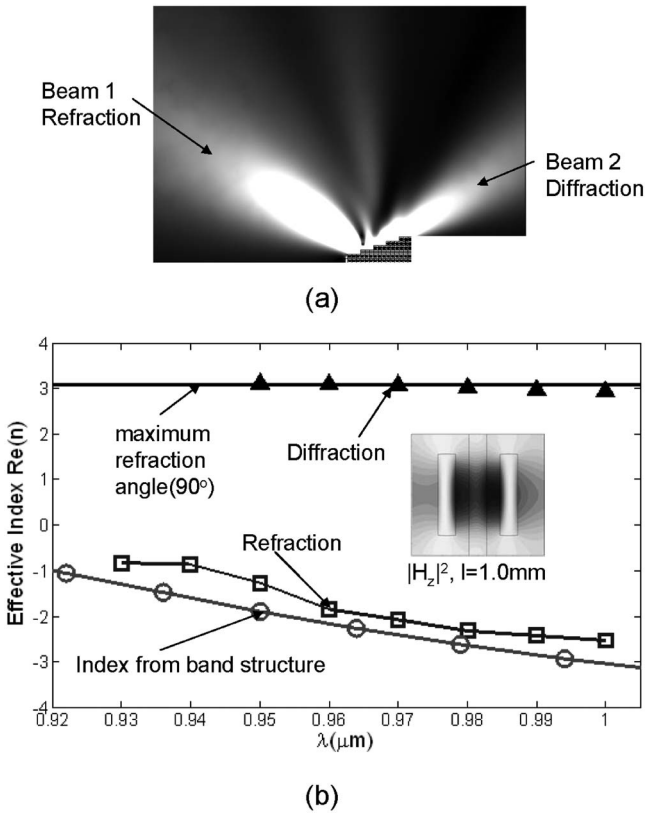

FIG. 3. (a) Time averaged power flow for a prism at an incident wavelength of $\lambda = 970$ nm. The dark background corresponds to nearly zero power flow. Disorder is introduced into the metal strip positions in the prism. Two far-field beams (1 and 2) are observed. (b) Comparison of effective indices extracted from numerical simulations and band structure calculations. Circles: Index calculated from the band structure of unit cell in Fig. 1(a). Squares: negative refraction. Triangles: diffraction. The horizontal line represents the angular position parallel to the hypotenuse. Inset: Amplitude of the magnetic field H_z of the Bloch mode of the unit cell in Fig. 1(a) at a wavelength of $\lambda = 1$ μm. Darker shade represents a larger field.

frequency dependences of the two beams reveal their respective physical origins: Beam 1 [Fig. 3(a)] corresponds to the refracted beam with its angular position consistent with predictions from Snell's law. This indicates that the negative refractive behavior is relatively insensitive to fabrication errors in the strip position and spacing. This insensitivity can be understood by inspection of the field profile of the plasmonic resonance, with its magnetic field concentrated between the two metal strips, as shown in the inset of Fig. 3(b). This resonance is responsible for the increased transmission in the negative index band. The resonances in neighboring unit cells are weakly coupled, and therefore insensitive to the disorder.

Beam 2 is a diffraction order that lies nearly parallel to the hypotenuse. As previously,[8] this diffraction order is due to the finite size of the small wedge. For a sufficiently large prism, this far-field beam will not be present.

In summary, a single layer of a subwavelength near-infrared NIM structure was fabricated. Its fabrication errors are shown to be within a range that preserves the negative index properties of the layers if employed in a bulk NIM. Moreover, a prism composed of the unit cells, where the paired metal strip positions are subject to random fabrication errors, are shown through numerical simulation to exhibit negative refraction despite these unavoidable variations. Our structure has a reduced in-plane periodicity and a comparable metal linewidth compared with split ring resonators,[11] and can be fabricated into a bulk NIM using an extension of the fabrication process described here. The structure also has a higher working frequency than the recently published stacked fishnet structure.[2]

The authors are grateful for discussions with Professor Anthony Grbic and Professor Roberto Merlin. We also thank the AFOSR MURI under Contract No. FA 9550-06-01-0279 for financial support.

[1] S. Zhang, W. J. Fan, N. C. Panoiu, K. J. Malloy, R. M. Osgood, and S. R. J. Brueck, Phys. Rev. Lett. **95**, 137404 (2005); V. M. Shalaev, W. S. Cai, U. K. Chettiar, H. K. Yuan, A. K. Sarychev, V. P. Drachev, and A. V. Kildishev, Opt. Lett. **30**, 3356 (2005).
[2] J. Valentine, S. Zhang, T. Zentgraf, E. Ulin-Avila, D. A. Genov, G. Bartal, and X. Zhang, Nature (London) **455**, 376 (2008).
[3] Y. A. Urzhumov and G. Shvets, Solid State Commun. **146**, 208 (2008).
[4] C. M. Soukoulis, J. F. Zhou, T. Koschny, M. Kafesaki, and E. N. Economou, J. Phys.: Condens. Matter **20**, 304217 (2008).
[5] S. Zhang, W. J. Fan, K. J. Malloy, S. R. J. Brueck, N. C. Panoiu, and R. M. Osgood, Opt. Express **13**, 4922 (2005).
[6] A. Mary, S. G. Rodrigo, F. J. Garcia-Vidal, and L. Martin-Moreno, Phys. Rev. Lett. **101**, 103902 (2008).
[7] V. Lomakin, Y. Fainman, Y. Urzhumov, and G. Shvets, Opt. Express **14**, 11164 (2006).
[8] X. H. Zhang, M. Davanco, Y. Urzhumov, G. Shvets, and S.R. Forrest, Phys. Rev. Lett. **101**, 267401 (2008).
[9] E. D. Palik, *Handbook of Optical Constants of Solids* (Academic, Orlando, 1985).
[10] M. Davanço, Y. Urzhumov, and G. Shvets, Opt. Express **15**, 9681 (2007).
[11] N. Liu, H. C. Guo, L. W. Fu, S. Kaiser, H. Schweizer, and H. Giessen, Nature Mater. **7**, 31 (2008).